Macromolecular Bioscience

Macromolecular Bioscience
www.mbs-journal.de

RESEARCH ARTICLE

Targeted Therapy for CD13-Overexpressing Triple-Negative Breast Cancers Using Apoptosis-Inducing Protein Cage Nanoparticles

Heejin Jun | Junsu Kim | Soomin Eom | Diane Jeong | Sebyung Kang

Department of Biological Sciences, Ulsan National Institute of Science and Technology (UNIST), Ulsan, Republic of Korea

Correspondence: Sebyung Kang (sabsab7@unist.ac.kr)

Received: 19 November 2025 | **Revised:** 25 January 2026 | **Accepted:** 28 January 2026

Keywords: CD13 | lumazine synthase | protein cage nanoparticles | TRAIL | triple negative breast cancer

ABSTRACT

Triple-negative breast cancer (TNBC) remains one of the most challenging breast cancer subtypes to treat due to the lack of well-defined molecular targets. Cluster of differentiation 13 (CD13), a cell surface aminopeptidase, is highly expressed in various tumors and play critical roles in promoting angiogenesis, aberrant proliferation, invasion, and metastasis. In this study, we investigated CD13 as a potential therapeutic target in TNBC cell lines to enable targeted therapy. Accordingly, we employed a protein cage nanoparticle, AaLS/TRAIL/aCD13Nb, which simultaneously displays CD13-binding nanobodies (aCD13Nb) and tumor necrosis factor-related apoptosis-inducing ligand (TRAIL) via the SpyCatcher/SpyTag protein ligation system. This dual-ligand nanoparticle exhibited enhanced and specific binding to CD13-overexpressing TNBC cell lines, including HCC1937, MDA-MB-468, and BT-549 cells. aCD13Nb-mediated tight binding facilitated sustained interaction of TRAIL with death receptors, resulting in robust activation of apoptotic signaling cascades and significantly enhanced therapeutic efficacy in CD13-overexpressing TNBC cell lines. Moreover, systemic administration of AaLS/TRAIL/aCD13Nb via intravenous injection markedly suppressed tumor growth in an HCC1937 xenograft mouse model, without evidence of systemic toxicity. These findings validate CD13 as a promising therapeutic target in TNBC and underscore the potential of dual-ligand protein cage nanoparticles as an effective platform for targeted cancer therapy.

1 | Introduction

Breast cancer is the most frequently diagnosed malignancy in women and remains a leading cause of cancer-related mortality worldwide [1]. Immunohistochemically, breast cancers are primarily classified based on the predominant expression of estrogen receptor (ER), progesterone receptor (PR), and human epidermal growth factor receptor 2 (HER2) [2]. The development of targeted therapies against these receptors has significantly improved treatment outcomes by enhancing treatment specificity and reducing off-target effects [3, 4]. However, triple negative breast cancer (TNBC), a subtype defined by the lack of ER, PR, and HER2, is associated with an aggressive clinical course and poorer prognosis compared to other breast cancer subtypes [5, 6]. Owing to the absence of targetable receptors, traditional chemotherapy has remained the mainstay of TNBC treatment for many years. However, the effectiveness of chemotherapy in TNBC is still limited by systemic toxicity and the frequent development

Heejin Jun and Junsu Kim contributed equally to this work.

of chemoresistance [7, 8]. Consequently, there is an urgent need to develop more effective and specific targeted therapies for TNBC that minimize adverse effects while improving clinical outcomes.

In recent years, extensive efforts to identify targetable receptors in TNBC have revealed several promising candidates, including epidermal growth factor receptor (EGFR), vascular endothelial growth factor (VEGF), and cluster of differentiation 13 (CD13) [9–12]. CD13, also known as aminopeptidase N (APN) or alanine aminopeptidase (AAP), is a transmembrane glycoprotein with protease activity [13, 14]. CD13 was initially characterized as a hematopoietic biomarker predominantly expressed on myeloid lineage cells, particularly in the context of acute myeloid leukemia (AML) [15–17]. It is also overexpressed in various solid tumors, including colon, prostate, liver, and breast cancers, where it serves as a valuable biomarker for diagnosis, prognosis, and potential therapeutic targeting [18, 19]. CD13 is known to play important roles in promoting angiogenesis, abnormal proliferation, invasion and metastasis [19]. A previous study reported a significant increase in CD13 activity in patients with breast cancer, highlighting its potential as a viable targetable antigen, particularly in TNBC [20].

Tumor necrosis factor-related apoptosis-inducing ligand (TRAIL), a member of the TNF superfamily, is a protein capable of inducing apoptosis when it binds to the specific receptors, death receptor 4 and 5 (DR4 and DR5) [21, 22]. Upon binding of TRAIL to death receptors, the death inducing signaling complex (DISC) is formed, leading to the activation of caspase-8, which subsequently triggers the activation of downstream effector caspases, including caspase-7, caspase-9, and caspase-3 [23]. Since cancer cells tend to overexpress DR4 and DR5 compared to normal cells, TRAIL is considered an effective cancer cell-specific apoptosis-inducing ligand [21, 24]. Despite its potent ability to induce cancer cell death, the in vivo application of soluble TRAIL faces several challenges, including short circulation half-life, low binding affinity to DR4/DR5 on cancer cell surfaces, and limited tumor-specific accumulation [22]. To overcome these challenges, we previously co-displayed TRAIL molecules and various tumor-targeting ligands on *Aquifex aeolicus* lumazine synthase (AaLS) protein cage nanoparticles using the SpyCather/SpyTag (SC/ST) protein ligation system [25–27]. The resulting dual-ligand-displaying protein cage nanoparticles effectively induced robust apoptotic cancer cell death both in vitro and in vivo. In particular, AaLS protein cage nanoparticles co-displaying TRAIL molecules and CD13-targeting nanobodies selectively bound to CD13-overexpressing AML cells, inducing robust apoptotic cell death. This targeted therapeutic strategy yielded a significant reduction in systemic AML burden in vivo and resulted in a marked extension of overall survival within the murine model [26]. The self-assembling AaLS protein cage nanoparticle consists of 60 subunits [28] and offers robust biostability, bioavailability, and versatility for functional modification [25–27, 29–33]. The SC/ST protein ligation system is derived from a split form of immunoglobulin-like collagen adhesion domain (CnaB2) from *Streptococcus pyogenes* [34]. The SC protein and ST peptide spontaneously form a covalent isopeptide bond, enabling stable and irreversible conjugation [34, 35]. Each component can be genetically fused to a diverse array of proteins while preserving the structural integrity and biological activity of the fusion partners [36–40].

In this study, we proposed a novel targeted therapeutic approach for TNBC using AaLS protein cage nanoparticles co-displaying TRAIL molecules and CD13-targeting nanobodies (AaLS/TRAIL/aCD13Nb) (Figure 1A). The expression levels of CD13 in various TNBC cell lines were initially evaluated by flow cytometry. The selective binding of AaLS/TRAIL/aCD13Nb to these TNBC cell lines was subsequently assessed in vitro using both flow cytometry and confocal microscopy. The in vitro cytotoxic efficacy of AaLS/TRAIL/aCD13Nb against various TNBC cell lines, in relation to their CD13 expression levels, was further evaluated using cell viability assay. In addition, activation of the TRAIL-mediated apoptotic pathway was assessed to elucidate the mechanism of action. Finally, a TNBC xenograft mouse model was established and used to evaluate the in vivo therapeutic potential of CD13-targeted, TRAIL-mediated treatment strategies in TNBC (Figure 1A). Overall, this work highlights the therapeutic potential of protein cage nanoparticles capable of co-displaying cancer-specific and pro-apoptotic ligands on a single platform, offering a promising strategy for the targeted treatment of TNBC.

2 | Results and Discussion

2.1 | Surface Expression Levels of CD13 and Death Receptors in TNBCs

As TNBCs lack well-defined targetable surface molecules, the identification of novel molecular targets is crucial for developing effective targeted therapies. Recent studies have highlighted CD13 as a potential candidate due to its emerging role in tumor progression and therapeutic resistance, as well as its overexpression in certain malignancies, including various breast cancer cells [41]. To initially investigate which TNBC cell lines express CD13, we conducted flow cytometry analysis using various breast cancer cell lines, including HCC1937, MDA-MB-468, BT549, MDA-MB-231, and MCF7 cells. High surface CD13 expression was observed in basal-like TNBC cell lines (HCC1937 and MDA-MB-468 cells) [42, 43] and in the mesenchymal-like TNBC cell line (BT549 cell) [44, 45] (Figure 1B,C). In contrast, another mesenchymal TNBC cell line (MDA-MB-231 cells) [44, 45] and the non-TNBC cell line (MCF7 cell) showed no detectable CD13 expression (Figure 1B,C).

Apoptosis is a regulated, non-inflammatory form of cell death, and TRAIL-based therapies selectively induce apoptosis in cancer cells while exhibiting minimal off-target effects on normal cells [21]. Since TRAIL molecules bind to death receptors (DRs) and subsequently induce apoptosis, we further measured the surface expression levels of death receptors in the tested cells (Figure 1B). Death receptor 5 (DR5) was highly expressed in MDA-MB-231 and MCF7 cells, moderately expressed in HCC1937 cells, and expressed at low levels in MDA-MB-468 and BT549 cells. In contrast, DR4 was barely expressed in all cell lines, except MDA-MB-231 cells. These findings suggest that the use of CD13-binding molecules for targeting, combined with TRAIL molecules as apoptosis-inducing ligands, could be a promising strategy for treating TNBCs, which lack readily targetable surface molecules.

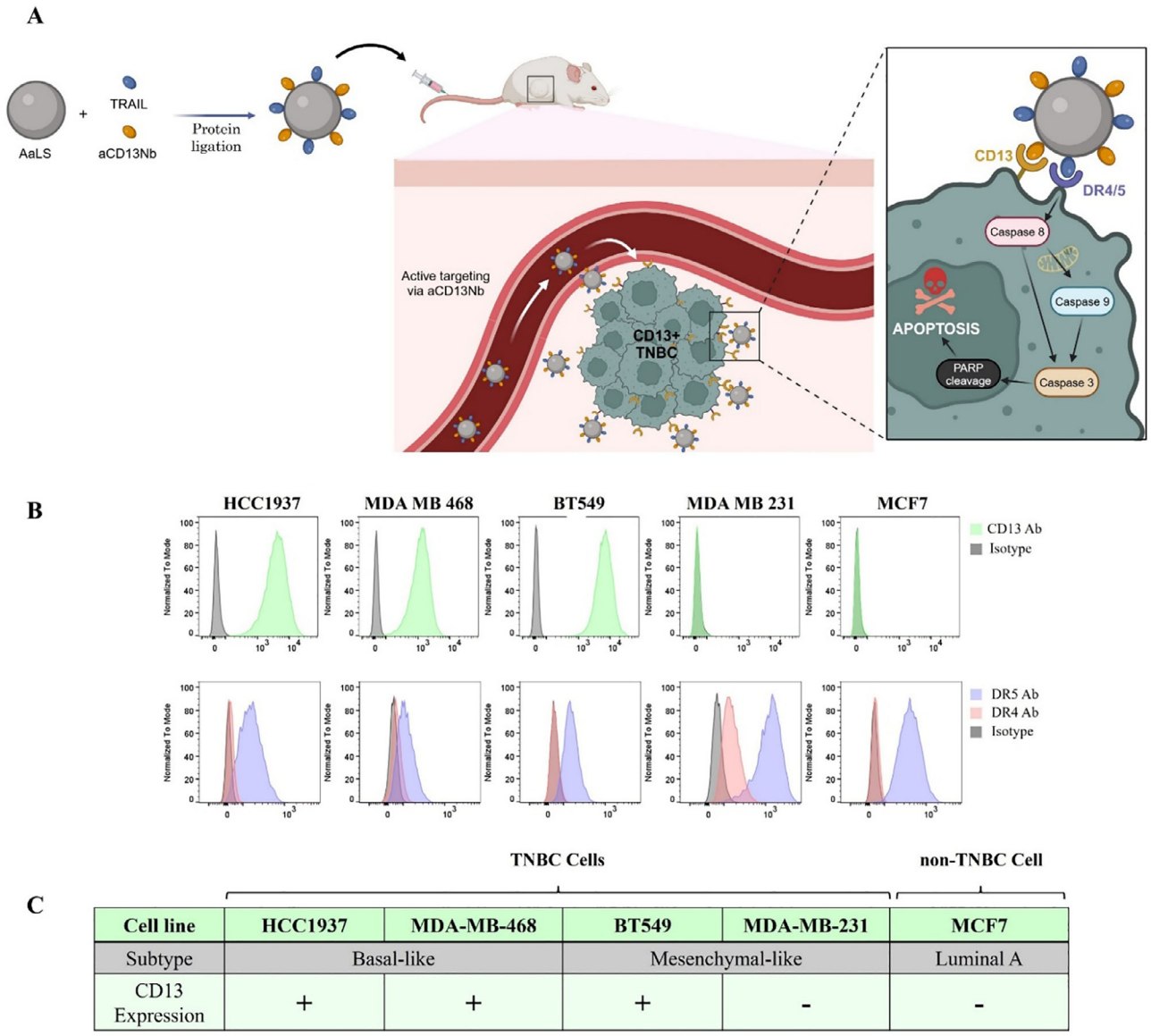

C

	TNBC Cells				non-TNBC Cell
Cell line	**HCC1937**	**MDA-MB-468**	**BT549**	**MDA-MB-231**	**MCF7**
Subtype	Basal-like		Mesenchymal-like		Luminal A
CD13 Expression	+	+	+	-	-

FIGURE 1 | Receptor expression levels of TNBC cells. (A) Schematic illustration of the protein cage nanoparticle-based targeted therapy for CD13-overexpressing TNBC cells (B) Flow cytometric analysis of HCC1937, MDA-MB-468, BT549, MDA-MB-231, and MCF7 cells treated with anti-CD13 antibody, anti-DR4 antibody, or anti-DR5 antibody. (C) Summary of CD13 surface expression levels in each cell line presented in tabular format.

2.2 | Construction of CD13-Targeting and TRAIL-Displaying AaLS Protein Cage Nanoparticles (AaLS/TRAIL/aCD13Nb)

For the treatment of CD13-overexpressing TNBCs, we utilized a previously constructed CD13-binding nanobody (aCD13Nb) [17, 26] as a targeting ligand and TRAIL as an apoptosis-inducing ligand. SpyCatcher (SC) was further genetically fused to aCD13Nb and TRAIL to create aCD13Nb-SC and SC-TRAIL, respectively. To display multiple TRAIL molecules and/or aCD13Nb, we prepared the previously established SpyTag (ST)-fused *Aquifex aeolicus* lumazine synthase protein cage nanoparticle (AaLS-ST) [30]. All recombinant proteins were overexpressed in *Escherichia coli* (*E. coli)* and purified in a single step using immobilized metal affinity chromatography (IMAC) with high purity (> 98 %) (Figure 2A, lane 2–4). Using purified proteins, TRAIL-displaying AaLS (AaLS/TRAIL), aCD13Nb-displaying AaLS (AaLS/aCD13Nb), and dual ligand-displaying AaLS (AaLS/TRAIL/aCD13Nb) variants were constructed using the SC/ST protein ligation system. Using a SC/ST post-translational protein-ligation system, we were able to control the amount of TRAIL and aCD13Nb on the AaLS-ST by modulating the input molar ratios of SC-TRAIL and aCD13Nb-SC onto the AaLS-ST subunit. To determine and control the relative amounts of displayed ligands on a AaLS protein cage nanoparticle, we conducted band intensity analyses of SDS-PAGE of individual proteins and ligated forms using the NIH Image J, which is one commonly used analytical technique to determine relative band intensities of multiple components in the SDS-PAGE [24]. Because each AaLS protein cage nanoparticle consists of 60 identical subunits, each AaLS-ST subunit is ligated to a single SC-fused protein (SC-TRAIL or aCD13Nb-SC), and the ratios among these subunits directly correspond to the number of ligands per particle, we were able to accurately determine both the final ligand composition and the number of each ligand

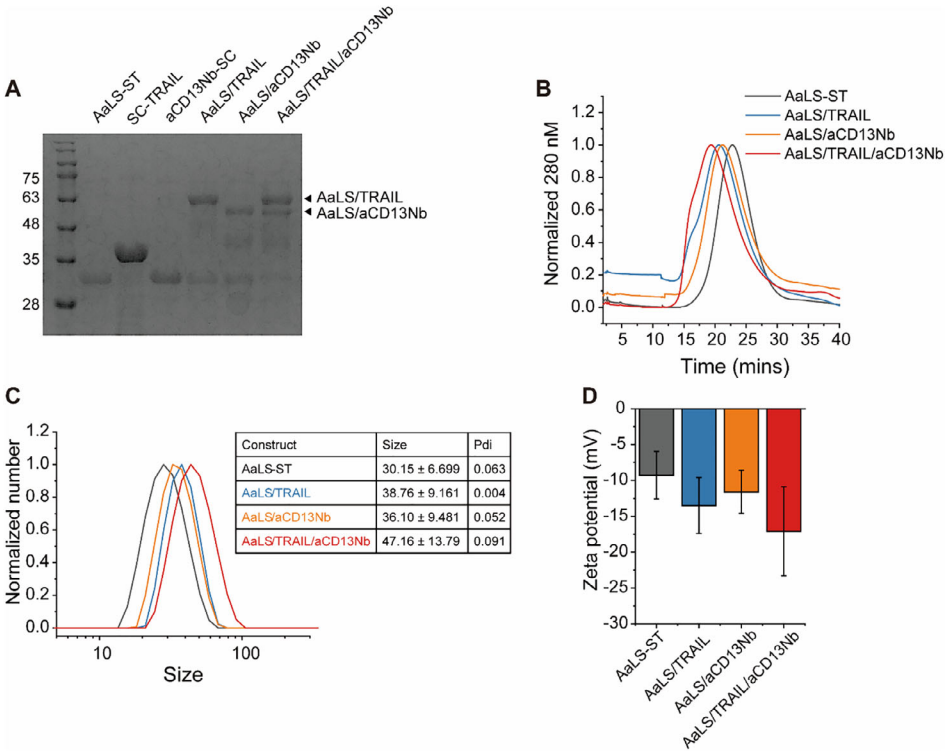

FIGURE 2 | Characterization of AaLS variants. (A) SDS-PAGE result of purified AaLS-ST, SC-TRAIL, and aCD13Nb-SC, and ligated AaLS variants. (B) Size exclusion chromatographic elution profiles of AaLS-ST, AaLS/TRAIL, AaLS/aCD13Nb, and AaLS/TRAIL/aCD13Nb. (C) DLS analysis and (D) Zeta-potentials of AaLS-ST, AaLS/TRAIL, AaLS/aCD13Nb, and AaLS/TRAIL/aCD13Nb (n = 3).

per particle. The covalent isopeptide bond formation between AaLS-ST subunits and SC-TRAIL or aCD13Nb-SC was confirmed by SDS-PAGE analysis (Figure 2A). AaLS-ST was mixed with each ligand (SC-TRAIL or aCD13Nb-SC) at a 2:1 molar ratio, resulting in complexes that displayed approximately 30 ligands per AaLS particle on average (Figure 2A, lane 5 & 6). When AaLS-ST was mixed with SC-TRAIL and aCD13Nb-SC at a 2:1:1 molar ratio, the resulting constructs simultaneously incorporated approximately 30 TRAIL molecules and 30 aCD13Nb molecules per AaLS particle on average (Figure 2A, lane 7). Size exclusion chromatography (SEC) was performed to monitor the elution profiles of the AaLS variants. AaLS/TRAIL/aCD13Nb eluted first, followed by AaLS/TRAIL, AaLS/aCD13Nb and AaLS-ST, demonstrating an increase in nanoparticle size upon ligand display (Figure 2B). The hydrodynamic diameters of AaLS-ST, AaLS/TRAIL, AaLS/aCD13Nb and AaLS/TRAIL/aCD13Nb were also measured using dynamic light scattering (DLS). Consistent with the SEC data, size increases were observed as 30.15, 38.76, 36.1, and 47.16 nm, respectively (Figure 2C). However, ligand display did not significantly alter the surface charges of the nanoparticles (Figure 2D). Taken together, these data confirm that the AaLS variants were successfully constructed while maintaining their protein cage architecture.

2.3 | Selective Binding of AaLS/TRAIL/aCD13Nb to CD13-Overexpressing TNBC Cell Lines

To examine the target-specific binding of ligand-displaying AaLS variants, the variants were labeled with fluorescein-5-maleimide (F5M) [30] and then incubated with the cells. Flow cytometry analysis revealed that aCD13Nb-displaying AaLS variants (AaLS/aCD13Nb and AaLS/TRAIL/aCD13Nb) strongly bound to the CD13-overexpressing TNBC cell lines, including HCC1937, MDA-MB-468 and BT549 cells (Figure 3A). In contrast, they did not bind to the CD13-negative TNBC cell line MDA-MB-231 or non-TNBC cell line MCF7 (Figure 3A), demonstrating their target-specific binding. A slight increase in fluorescent signal was observed in HCC1937, MDA-MB-231, and MCF7 cells treated with AaLS/TRAIL (Figure 3A), probably due to the higher surface expression of DR5 on these cells compared to MDA-MB-468 and BT549 cells (Figure 1B). Furthermore, laser scanning confocal microscopy imaging was performed on HCC1937 cells following treatment with AaLS variants. AaLS/aCD13Nb and AaLS/TRAIL/aCD13Nb exhibited strong membrane surface binding to HCC1937 cells (Figure 3B), consistent with the flow cytometry data (Figure 3A). In contrast, binding of AaLS/TRAIL was not detected in the confocal images, likely due to the weak binding affinity of TRAIL for DRs. These results imply that the aCD13Nb component of AaLS/TRAIL/aCD13Nb specifically targets CD13 on the surface of TNBC cells, highlighting its potential as a promising strategy for targeted therapy against CD13-overexpressing TNBCs.

2.4 | Enhanced Apoptotic Cell Death of CD13-Overexpressing TNBC Cell Lines With AaLS/TRAIL/aCD13Nb

Given the urgent need for targeted therapies in TNBCs, we aimed to investigate the potential of CD13-targeted therapy by evaluating the therapeutic efficacy of AaLS/TRAIL/aCD13Nb.

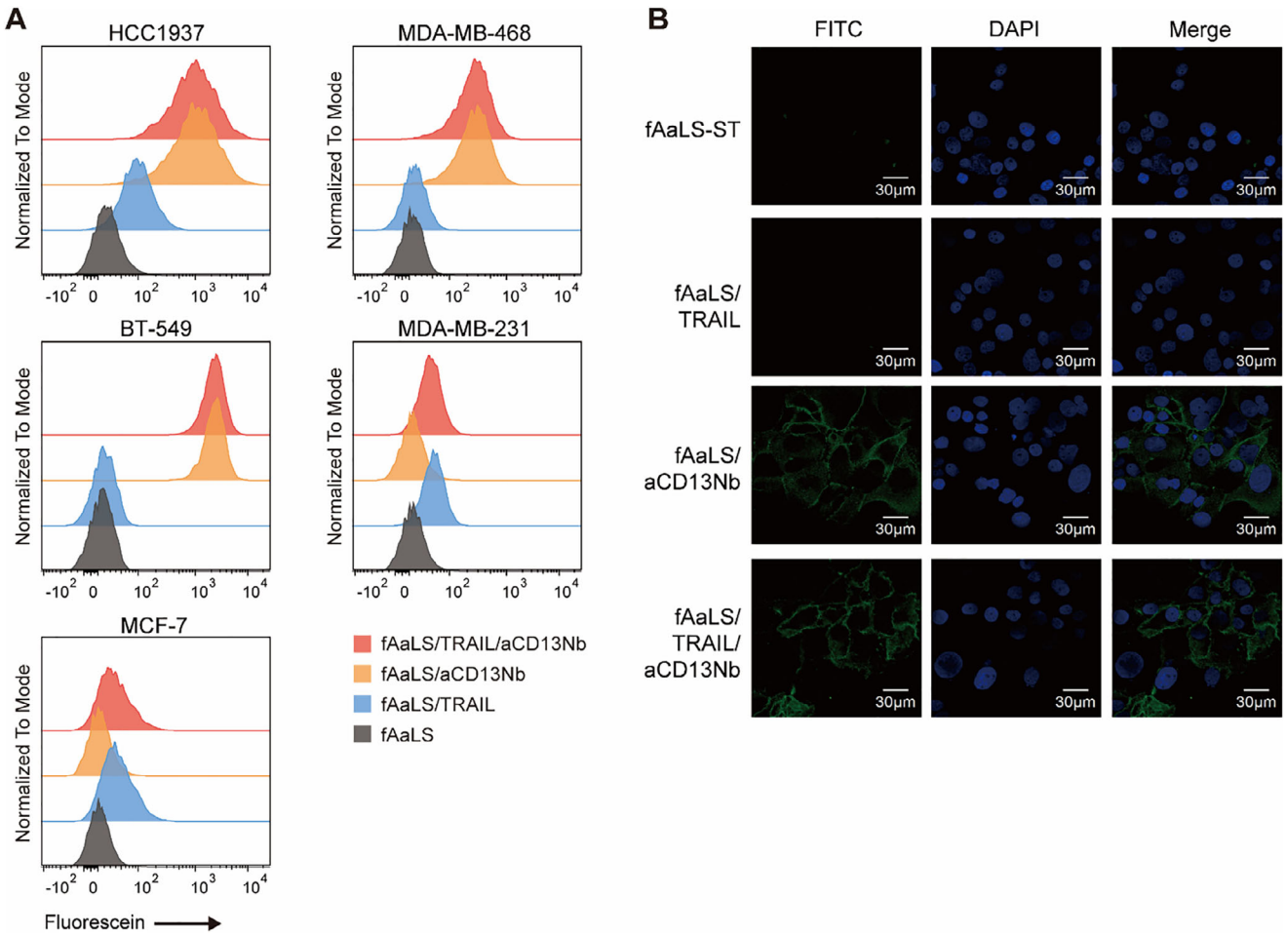

FIGURE 3 | aCD13Nb-mediated selective binding of AaLS variants to various breast cancer cell lines. (A) Flow cytometric analysis of HCC1937, MDA-MB-468, BT549, MDA-MB-231, and MCF-7 cells treated with fAaLS-ST, fAaLS/aCD13Nb, fAaLS/TRAIL, or fAaLS/TRAIL/aCD13Nb. (B) Fluorescent microscopic images of HCC1937 cells treated with fAaLS-ST, fAaLS/aCD13Nb, fAaLS/TRAIL, or fAaLS/TRAIL/aCD13Nb. Scale bar = 30 μm.

CD13-overexpressing TNBC cell lines (HCC1937, MDA-MB-468, and BT549 cells), CD13-negative TNBC cells (MDA-MB-231), and CD13-negative non-TNBC cells (MCF7) were treated with AaLS-ST, AaLS/aCD13Nb, AaLS/TRAIL, or AaLS/TRAIL/aCD13Nb for 24 h, and cell viability was assessed using the CCK-8 assay (Figure 4A). CD13-targeted therapy demonstrated significant promise, as AaLS/TRAIL/aCD13Nb exhibited enhanced cytotoxicity in HCC1937, MDA-MB-468, and BT549 cells compared to AaLS/TRAIL. Notably, HCC1937 cells showed resistance to high concentrations (100 nM) of AaLS/TRAIL, but this resistance was substantially overcome by the presence of aCD13Nb, highlighting its essential role in enhancing TRAIL-mediated apoptosis. In contrast, in CD13-negative TNBC MDA-MB-231 cells, AaLS/TRAIL and AaLS/TRAIL/aCD13Nb showed nearly identical cytotoxicity (Figure 4A). The non-TNBC MCF7 cells which are known to highly resistant to TRAIL, showed no cytotoxicity with both AaLS/TRAIL and AaLS/TRAIL/aCD13Nb (Figure 4A). Despite high CD13/DR5 expression and superior binding of the AaLS/TRAIL/aCD13Nb complex, BT549 cell viability plateaus at approximately 40%. This may reflect impairment of the downstream apoptotic cascade due to anti-apoptotic mechanisms acting on TRAIL-mediated signaling [46–48]. To further investigate whether the enhanced cytotoxicity of AaLS/TRAIL/aCD13Nb against CD13-overexpressing TNBC cells results from TRAIL/DR-mediated and caspase-dependent apoptosis pathways, we examined caspase-dependent apoptotic signaling in HCC1937 and MDA-MB-468 cells treated with 1 nM AaLS variants for 4 h. This representative concentration was selected because AaLS/TRAIL/aCD13Nb induced strong cytotoxicity, whereas AaLS/TRAIL did not, in both HCC1937 and MDA-MB-468 cells (Figure 4A). Western blot analysis revealed significant cleavage of key apoptotic signaling markers, including caspase-8, caspase-9, caspase-3, and PARP, in AaLS/TRAIL/aCD13Nb-treated cells (Figure 4B; Figure S1A). In contrast, AaLS/TRAIL treatment induced only slight activation of caspase-9, caspase-3, and PARP in HCC1937 cells (Figure 4B), and a slight activation of PARP in MDA-MB-468 cells (Figure S1A). Neither AaLS-ST nor AaLS/aCD13Nb triggered detectable apoptotic signaling, which aligns well with the cytotoxicity assay results showing that neither variant affected cell viability (Figure 4A; Figure S1A). Furthermore, treatment of HCC1937 cells with IC_{50} concentrations of AaLS/TRAIL (100 nM) and AaLS/TRAIL/aCD13Nb (0.75 nM) resulted in a similar cleavage pattern of apoptotic signaling markers (Figure S1B). These results indicate that the enhanced cytotoxicity of AaLS/TRAIL/aCD13Nb is mediated by amplified TRAIL-induced apoptotic cell death through strong aCD13Nb-mediated nanoparticle binding.

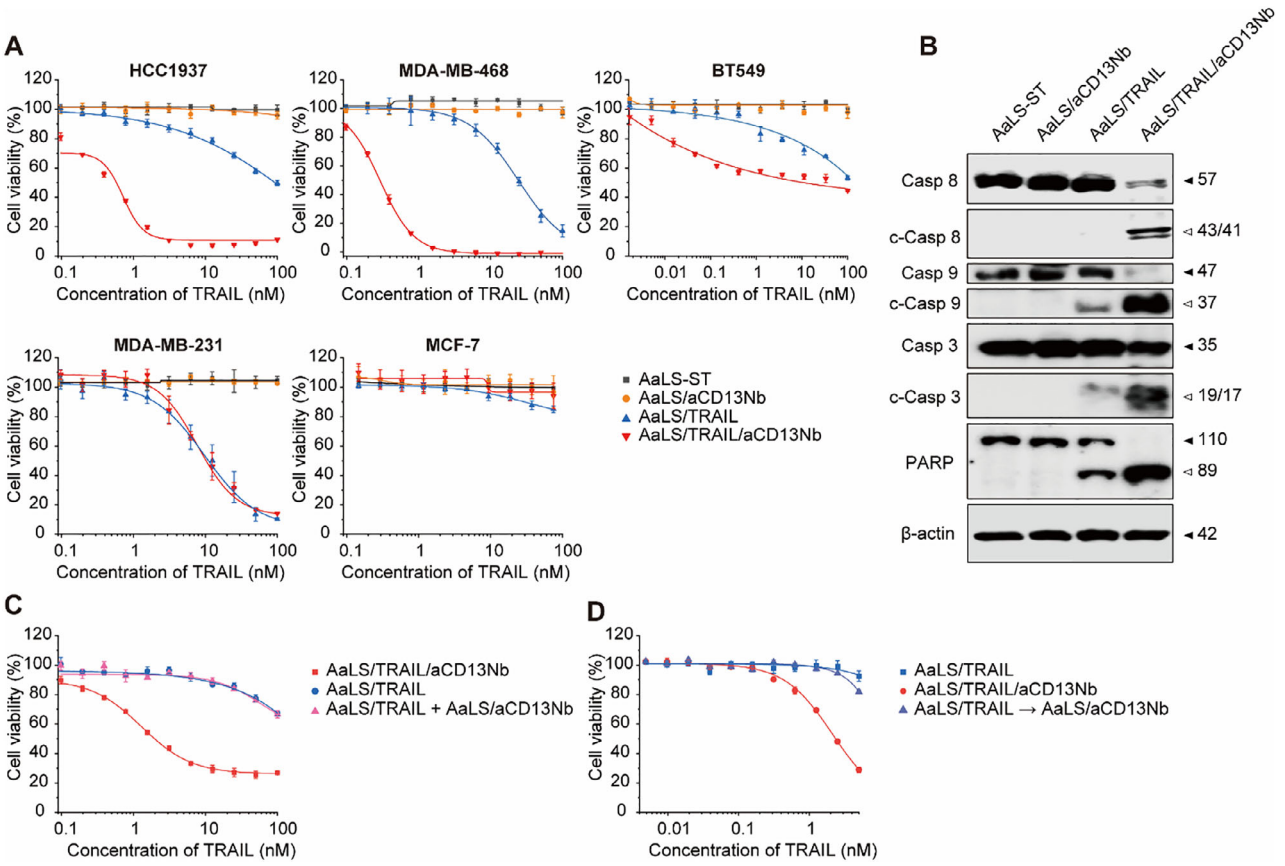

FIGURE 4 | Cytotoxic effects of AaLS variants in breast cancer cell lines. (A) In vitro dose-dependent cytotoxicity of AaLS-ST, AaLS/aCD13Nb, AaLS/TRAIL, or AaLS/TRAIL/aCD13Nb in HCC1937, MDA-MB-468, BT549, MDA-MB-231 and MCF7 cells, as determined using a CCK-8 assay. All data shown in (A) are means ± standard deviation (SD); n = 3. (B) Western blot analysis of DR-mediated apoptotic signals. HCC1937 cells were treated with 1 nM AaLS-ST, AaLS/aCD13Nb, AaLS/TRAIL, or AaLS/TRAIL/aCD13Nb. β-actin was used as a loading control. (C) In vitro dose-dependent cytotoxicity of AaLS/TRAIL, AaLS/TRAIL/aCD13Nb or co-treatment of AaLS/TRAIL and AaLS/aCD13Nb to HCC1937 cells as determined by a CCK8 assay. (B) In vitro dose-dependent cytotoxicity of AaLS/TRAIL, AaLS/TRAIL/aCD13Nb, or a pre-treatment of AaLS/aCD13Nb for 30 min, followed by treatment with AaLS/TRAIL/aCD13Nb. All data are means ± standard deviation (SD); $n = 3$.

To determine whether the co-display of aCD13Nb and TRAIL on the same nanoparticle is essential for enhancing therapeutic efficacy in CD13-overexpressing TNBC cells, we assessed the cytotoxicity of a simple mixture of AaLS/TRAIL and AaLS/aCD13Nb in HCC1937 cells and compared it with that of AaLS/TRAIL and AaLS/TRAIL/aCD13Nb. A simple mixture of AaLS/TRAIL and AaLS/aCD13Nb showed cytotoxicity nearly identical to that of AaLS/TRAIL alone, whereas AaLS/TRAIL/aCD13Nb exhibited significantly enhanced cell-killing activity (Figure 4C). Furthermore, pre-treatment with an excess amount of AaLS/aCD13Nb (50 nM) prior to AaLS/TRAIL/aCD13Nb significantly reduced cytotoxicity compared to treatment with AaLS/TRAIL/aCD13Nb alone (Figure 4D). These results suggest that pre-bound AaLS/aCD13Nb on CD13 molecules at the TNBC cell surface likely inhibits the tight binding of AaLS/TRAIL/aCD13Nb to TNBC cells, thereby competing for CD13 and hindering efficient interactions between TRAIL and DRs, ultimately blocking TRAIL-mediated apoptosis. Collectively, these results highlight the therapeutic potential of CD13-targeted therapy for TNBC, demonstrating that the enhanced cytotoxicity of AaLS/TRAIL/aCD13Nb is primarily driven by the specific and strong interaction between aCD13Nb and CD13. This interaction facilitates sustained and consistent TRAIL/DR engagement, ultimately promoting robust apoptosis in CD13-overexpressing TNBC cells.

2.5 | Outstanding Therapeutic Efficacy of AaLS/TRAIL/aCD13Nb Against TNBC HCC1937 Tumors In Vivo

To evaluate the therapeutic potential of CD13-targeted therapy in CD13-overexpressing TNBC cells in vivo, an HCC1937 tumor-xenografted mouse model was established. When the HCC1937 tumors reached approximately 100 mm^3, the mice were intravenously injected with PBS, AaLS/TRAIL, AaLS/aCD13Nb, AaLS/TRAIL/aCD13Nb, or SC-TRAIL every 3 or 4 days. Compared to the PBS-treated group, treatment with AaLS/TRAIL/aCD13Nb resulted in significant inhibition of tumor growth (Figure 5A; Figure S2). In contrast, AaLS/TRAIL exhibited only modest tumor suppression relative to AaLS/TRAIL/aCD13Nb. Although AaLS/aCD13Nb bound well to HCC1937 cells (Figure 3), it did not reduce tumor growth compared to the PBS-treated group, likely due to its inability to induce apoptosis (Figure 5A). On day 32, HCC1937 tumors and major organs were excised from sacrificed mice for further

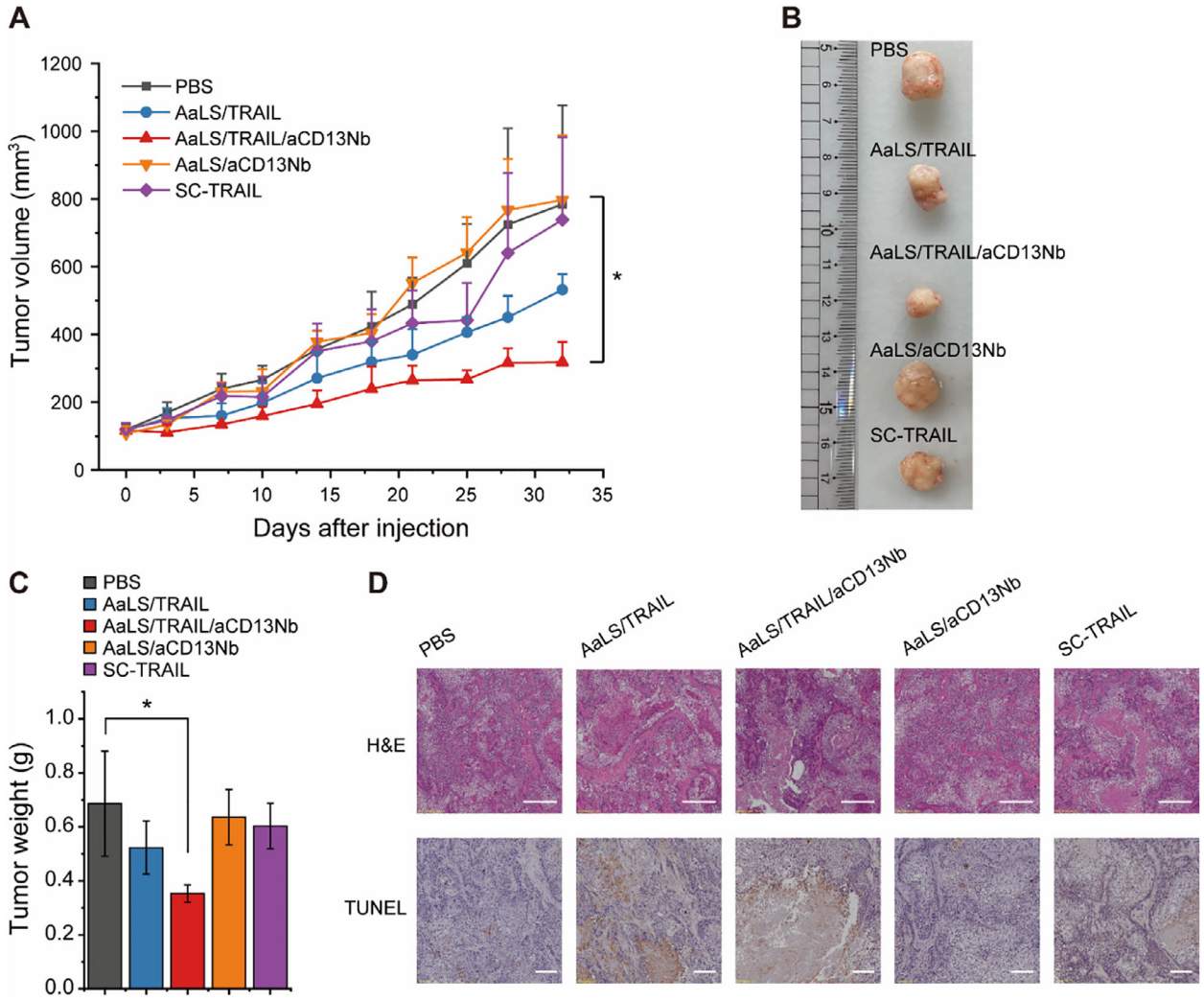

FIGURE 5 | In vivo antitumor activity of AaLS variants in an HCC1937 xenograft model. (A) Tumor growth curves of HCC1937 tumor xenografted mice treated with PBS, AaLS/TRAIL, AaLS/TRAIL/aCD13Nb, AaLS/aCD13Nb, or SC-TRAIL. The data are averages ± standard deviation (SD); n = 4 per group; *p*-value is adjusted for multiple comparisons; *$p < 0.05$. (B) Representative images of excised tumors from mice treated with PBS, AaLS/TRAIL, AaLS/TRAIL/aCD13Nb, AaLS/aCD13Nb or SC-TRAIL. (C) Tumor weights of excised tumors from each treatment group. (D) Representative H&E and TUNEL staining images of tumor sections collected from treated mice. Scale bar = 500 μm (H&E) and 200 μm (TUNEL).

analysis. The images and measured tumor weights from each group (Figure 5B,C) showed that the AaLS/TRAIL/aCD13Nb treatment group had the smallest tumor size and weight, consistent with the tumor volume measurement (Figure 5A). Additionally, histopathological staining of the excised tumors was performed to confirm that tumor growth inhibition resulted from TRAIL-mediated apoptosis. Hematoxylin and eosin (H&E) staining revealed significant nuclear dissociation in the AaLS/TRAIL/aCD13Nb-treated group compared to the PBS- or AaLS/aCD13Nb-treated groups (Figure 5D). The AaLS/TRAIL- and SC-TRAIL-treated groups also exhibited nuclear dissociation, although to a lesser extent. Terminal deoxynucleotidyl transferase-mediated dUTP nick end labeling (TUNEL) staining showed a similar trend in apoptosis. Among all groups, AaLS/TRAIL/aCD13Nb treatment resulted in the largest area of TUNEL-positive cells, indicating potent apoptosis-mediated tumor suppression. A moderate TUNEL-positive area was observed in the AaLS/TRAIL-treated group, while the SC-TRAIL-treated group exhibited the smallest (Figure 5D). Collectively, these results demonstrate the superior therapeutic efficacy of AaLS/TRAIL/aCD13Nb.

To evaluate the in vivo safety of the current approach, we monitored mouse body weights, assessed tissue damage in major organs, and evaluated organ function. No significant fluctuations in total body mass were recorded across any treatment groups, suggesting a favorable safety profile (Figure 6A). H&E staining of major organs, including the heart, kidney, liver, lung and spleen, showed no significant pathological damage in any treatment group (Figure 6B). Furthermore, the levels of aspartate aminotransferase (AST) activity, alanine transaminase (ALT) activity, and creatinine were not altered following treatment with AaLS/TRAIL/aCD13Nb, clearly indicating that liver and kidney functions remained normal in the mice (Figure 6C). Taken together, the therapeutic efficacy of CD13-targeted TRAIL delivery using protein cage nanoparticles against CD13-overexpressing TNBC was clearly demonstrated in vivo, successfully inducing apoptotic cell death in tumor cells without causing significant

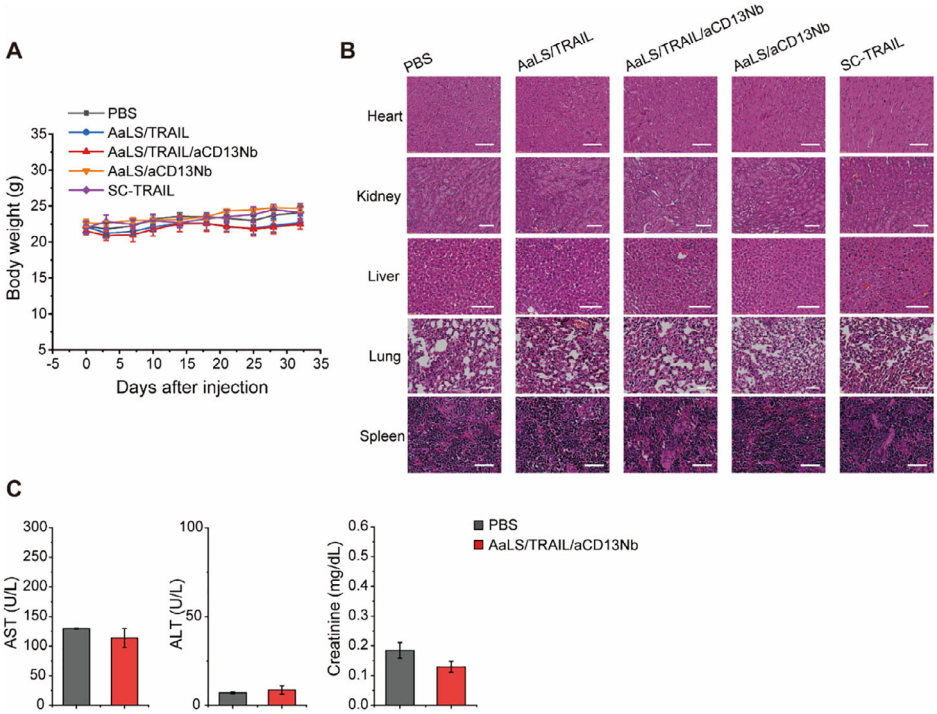

FIGURE 6 | In vivo safety assessment of AaLS variant therapy. (A) Body weights of mice treated with PBS, AaLS/TRAIL, AaLS/TRAIL/aCD13Nb, AaLS/aCD13Nb or SC-TRAIL. (B) H&E staining images of major organs collected from mice in each treatment group. Scale bar = 100 μm (Heart, Kidney, Liver) and 50 μm (Lung, Spleen). (C) Serum levels of ALT, AST, and creatinine in mice from each treatment group. Data are represented as means ± SD, n = 4.

toxicity in major organs. These findings underscore the potential of CD13 as a promising surface marker for TNBC diagnosis and treatment, as well as the potential to expand the current approach to treat other cancers that may not have specific biomarkers but potentially express CD13 on their surface.

3 | Conclusions

TNBC is a recalcitrant breast cancer subset characterized by a deficient expression of key surface biomarkers, including ER, PR, and HER2, which limits the effectiveness of conventional targeted therapies. To address this challenge, we investigated CD13 as a potential surface biomarker for TNBC. Flow cytometry analysis showed that CD13 was highly expressed in several TNBC cell lines, including HCC1937, MDA-MB-468, and BT549 cells, but was low or absent in MDA-MB-231 cells and in the non-TNBC MCF-7 cells. To selectively target and induce apoptosis in CD13-overexpressing TNBC cells, we employed a previously designed dual ligand-displaying protein cage nanoparticle which co-displays both aCD13Nb and TRAIL molecules using the SC/ST protein ligation system. This strategy allowed for the stable and simultaneous presentation of both ligands on the surface of the AaLS protein cage nanoparticles, resulting in the formation of AaLS/TRAIL/aCD13Nb.

AaLS/TRAIL/aCD13Nb exhibited selective binding to CD13-overexpressing TNBC cell lines, confirming aCD13Nb-mediated target specificity. While the cytotoxicity of AaLS/TRAIL varied across cell lines, AaLS/TRAIL/aCD13Nb showed markedly enhanced cytotoxicity in CD13-overexpressing TNBC cells. Mechanistically, AaLS/TRAIL/aCD13Nb strongly activated death receptor signaling, leading to subsequent caspase activation, PARP cleavage, and apoptotic cell death. However, pretreatment of HCC1937 cells with AaLS/aCD13Nb attenuated the cytotoxic effects of AaLS/TRAIL/aCD13Nb, and a simple mixture of AaLS/TRAIL and AaLS/aCD13Nb exhibited cytotoxicity nearly identical to that of AaLS/TRAIL alone, confirming the CD13-dependence of AaLS/TRAIL/aCD13Nb's therapeutic activity. This enhanced cytotoxicity was attributed to the tight binding of aCD13Nb to CD13, which facilitated sustained TRAIL-mediated apoptosis.

In a HCC1937 tumor xenograft mouse model, treatment with AaLS/TRAIL/aCD13Nb significantly suppressed tumor growth without inducing significant side effects. Collectively, our study validates CD13 as a viable therapeutic target in a subset of TNBCs and showed potential of AaLS/TRAIL/aCD13Nb as a safe and effective targeted treatment strategy for CD13-overexpressing TNBCs.

4 | Materials and Methods

4.1 | Purification of Proteins

The genes encoding AaLS-ST subunit with an R108C point mutation and SC-TRAIL in the pETduet-1 vector, as well as aCD13Nb-SC in the pET30b vector, were previously constructed and used in this study without modification [25, 26]. Recombinant proteins were overexpressed as previously described [24, 25] and purified using an immobilized metal affinity chromatography

(IMAC) [30]. Following chromatographic purification, purified protein fractions were equilibrated into a phosphate-buffered saline (PBS) environment via dialysis, ensuring compatibility with subsequent in vitro and in vivo assays.

4.2 | Cell Lines

Human breast cancer cell lines, HCC1937, MDA-MB-468, BT549, MDA-MB-231, and MCF-7 cells, were purchased from ATCC and cultured under 37°C and 5% CO_2 condition. HCC1937, BT549, and MCF-7 were maintained in RPMI-1640 medium (Gibco), while MDA-MB-468 and MDA-MB-231 cells were propagated in Dulbecco's Modified Eagle Medium (DMEM; Gibco). All basal media were supplemented with 10% (v/v) heat-inactivated fetal bovine serum (FBS; Gibco) and 1% (v/v) antibiotic-antimycotic solution (Gibco).

4.3 | Flow Cytometry Analysis of Membrane Protein Levels in Human Breast Cancer Cell Lines

To evaluate cell surface expression of CD13 in human breast cancer cell lines, 5×10^5 cells of HCC1937, MDA-MB-468, BT549, MDA-MB-231, or MCF-7 cells were rinced twice with ice-cold PBS and subsequently treated with either an isotype control or anti-CD13 antibody (14-0138-82, Invitrogen) in a blocking matrix of 3% BSA in PBS. Following a 30-min incubation at 4°C, excess primary antibody was removed via three successive PBS washes. The cells were then treated with an Alexa Fluor-conjugated anti-mouse IgG secondary antibody (A-11001, Invitrogen) in blocking buffer for 30 min at 4°C, protected from light. The cells were then washed three more times with ice-cold PBS, and CD13 surface expression was analyzed using flow cytometry (BD LSR fortessa). To evaluate cell surface expression of DR4 and DR5 in human breast cancer cell lines, 5×10^5 cells of HCC1937, MDA-MB-468, BT549, MDA-MB-231, or MCF-7 cells were rinsed twice with ice-cold PBS and treated with either an isotype control, PE-conjugated anti-DR4 antibody (12-6644-42, Invitrogen), or PE-conjugated anti-DR5 antibody (12-9908-41, Invitrogen) in blocking buffer for 30 min at 4°C, protected from light. The cells were rinsed three times with ice-cold PBS to thoroughly remove non-specific antibodies. Subsequently, DR4 and DR5 surface expression was analyzed using flow cytometry.

4.4 | Binding Assay of AaLS Variants to TNBC Cell Lines

Fluorescently labeled AaLS-ST (fAaLS-ST) was prepared by conjugating the cysteine residue at position 108 of the AaLS-ST subunits with fluoresceine-5-maleimide (F5M, Thermo Fisher Scientific) via thiol-maleimide Michael addition [49]. Unreacted free F5M molecules were removed by dialysis. Subsequently, SC-TRAIL, aCD13Nb-SC, or both were ligated to fAaLS-ST via the SC/ST ligation system to generate fAaLS/aCD13Nb, fAaLS/TRAIL, or fAaLS/TRAIL/aCD13Nb. 5×10^5 cells of HCC1937, MDA-MB-468, BT549, MDA-MB-231, or MCF-7 cells were rinsed twice with ice-cold PBS and incubated with fAaLS-ST, fAaLS/aCD13Nb, fAaLS/TRAIL or fAaLS/TRAIL/aCD13Nb for 30 min at 4°C, protected from light. The cells were rinsed three times with ice-cold PBS to completely remove the non-specific samples. Subsequently, cellular fluorescence intensities were acquired using a flow cytometer.

4.5 | Fluorescence Microscopic Imaging

4×10^5 cells of HCC1937 were seeded on the microscope cover glass in a 12-well plate overnight. The cells were fixed with 4% paraformaldehyde (PFA) in PBS for 30 min at room temperature and washed three times with PBS. The cells were then treated with blocking buffer (5% BSA and 0.1% Triton X-100 in PBS), incubated for 30 min at room temperature, and incubated with fAaLS-ST, fAaLS/aCD13Nb, fAaLS/TRAIL or fAaLS/TRAIL/aCD13Nb at room temperature for 30 min, protected from light. The cells were rinsed three times with PBS to completely remove the unbound samples. The nuclei were stained with DAPI and images of the samples were obtained using an Olympus Fluoview FV100 fluorescent microscope (Olympus, UOBC).

4.6 | Cell Viability Test

7×10^3 cells of HCC1937, MDA-MB-468, BT549, MDA-MB-231, or MCF-7 cells were seeded into each well of a 96 well plate (Eppendorf) and incubated with AaLS-ST, AaLS/TRAIL, AaLS/aCD13Nb, or AaLS/TRAIL/aCD13Nb (starting concentration: 100 nM) via a two-fold serial dilution for 24 h in complete growth medium. Cell viability was quantified using the Cell Counting Kit-8 (CCK-8, Dojindo) colorimetric assay, following the manufacturer's established protocol.

4.7 | Western Blot

HCC1937 and MDA-MB-468 cells were rinsed twice in PBS and subsequently lysed in IP lysis buffer (Thermo Fisher Scientific) containing 1% protease and phosphatase inhibitors cocktail (Thermo Fisher Scientific). The lysates were clarified by centrifugation at 13 000 rpm for 15 min at 4°C, and protein concentrations were determined using the Pierce BCA Protein Assay Kit (Thermo Fisher Scientific), following the manufacturer's established protocol. Equal amounts of protein were mixed with 5 × SDS-PAGE sample loading buffer (250 mM Tris-HCl, pH 6.8, 0.5 M DTT, 10% SDS, 50% Glycerol, 0.2% Bromophenol blue), followed by boiling at 95°C for 5 min. Proteins were resolved by SDS-PAGE and subsequently electroblotted onto an Immuno-Blot polyvinylidene fluoride (PVDF) membrane (BIO-RAD). After blocking non-specific binding with 5% BSA in Tris-buffered saline with 0.1% Tween-20 (TBST) for 1 h at room temperature, membranes were incubated overnight at 4°C with the following primary antibodies: anti-caspase-8 (Cell Signaling Technology, #9746), anti-caspase-3 (Cell Signaling Technology, #9662), anti-caspase-9 (Cell Signaling Technology, #9237) anti-PARP (Cell Signaling Technology, #9542), anti-β-actin (Thermo Fisher scientific, MA1-140). The membranes were then washed three times with TBST and incubated with horseradish peroxidase (HRP)-conjugated secondary antibodies (Jackson ImmunoResearch) for 1 h at room temperature. Protein bands were visualized using enhanced chemiluminescence (ECL) reagents (GE healthcare).

4.8 | In Vivo Anti-Tumor Efficacy Test

All animal studies and procedures were approved by the guidance of the Institutional Animal Care and Use Committee of the Ulsan National Institute of Science and Technology (UNISTIACUC-24-67). NOD-scid IL2Rgamma^{null} (NSG) mice (5–7-week-old; Jackson Laboratory) were subcutaneously injected with 100 μL of 3×10^6 HCC1937 cells to establish a tumor xenograft model. Once the average tumor volume reached approximately 150 mm^3, mice were randomly distributed to different treatment groups (n = 4 per group) and received intravenous injections of either PBS, AaLS/aCD13Nb (11 mg/kg), SC-TRAIL (5 mg/kg), AaLS/TRAIL (12 mg/kg), or AaLS/TRAIL/aCD13Nb (14 mg/kg) every 3 to 4 days for a total of seven injections.

4.9 | In Vivo Safety Assessment

To assess the hepatotoxic potential of the treatment, serum concentrations of aspartate aminotransferase (AST) and alanine aminotransferase (ALT) were quantified 24 h after intravenous injection of AaLS/TRAIL/aCD13Nb. Whole blood was harvested via terminal cardiac puncture, and serum was subsequently partitioned through centrifugation. AST and ALT activities were quantified using the Aspartate Aminotransferase Activity Assay Kit (Abcam) and Alanine Transaminase Activity Assay Kit (Colorimetric/fluorometric, Abcam), respectively, following the manufacturer's instructions. To assess kidney function, serum creatinine levels were quantified using the Creatinine Assay Kit (Sigma-Aldrich), following the manufacturer's protocol.

4.10 | Statistical Analysis

All data are presented as mean ± standard deviation (SD) from at least three independent experiments. Statistical analyses were performed using student's *t*-test or two-way analysis of variance (ANOVA). *p*-values less than 0.05 were considered statistically significant and are indicated as follows: $p \leq 0.05$ (*), $p \leq 0.01$ (**), $p \leq 0.001$ (***), $p \leq 0.0001$ (****).

Acknowledgements

This work was supported by the National Research Foundation of Korea (RS-2018-NR031072 and RS-2025-23323382) funded by the Korean Government. We thank UNIST Office of Research Facilities and Training (ResFacT) for support of using the equipment.

Funding

This work was supported by the National Research Foundation of Korea (RS-2018-NR031072 and RS-2025-23323382) funded by the Korean Government.

Conflicts of Interest

The authors declare no conflict of interest.

Data Availability Statement

The data that support the findings of this study are available from the corresponding author upon reasonable request.

References

1. H. Sung, J. Ferlay, R. L. Siegel, et al., "Global Cancer Statistics 2020: Globocan Estimates of Incidence and Mortality Worldwide for 36 Cancers in 185 Countries," *CA: A Cancer Journal for Clinicians* 71 (2021): 209–249.

2. A. A. Onitilo, J. M. Engel, R. T. Greenlee, and B. N. Mukesh, "Breast Cancer Subtypes Based on ER/PR and HER2 Expression: Comparison of Clinicopathologic Features and Survival," *Clinical Medicine & Research* 7 (2009): 4–13, https://doi.org/10.3121/cmr.2008.825.

3. M. J. Higgins and J. Baselga, "Targeted Therapies for Breast Cancer," *Journal of Clinical Investigation* 121 (2011): 3797–3803, https://doi.org/10.1172/JCI57152.

4. S. M. Swain, M. Shastry, and E. Hamilton, "Targeting HER2-Positive Breast Cancer: Advances and Future Directions," *Nature Reviews Drug Discovery* 22 (2023): 101–126, https://doi.org/10.1038/s41573-022-00579-0.

5. W. J. Irvin Jr and L. A. Carey, "What is Triple-Negative Breast Cancer?," *European Journal of Cancer* 44 (2008): 2799–2805, https://doi.org/10.1016/j.ejca.2008.09.034.

6. T. Ovcaricek, S. G. Frkovic, E. Matos, et al., "Triple Negative Breast Cancer-Prognostic Factors and Survival," *Radiology and Oncology* 45 (2011): 46–52.

7. G. Bianchini, C. De Angelis, L. Licata, and L. Gianni, "Treatment Landscape of Triple-Negative Breast Cancer — Expanded Options, Evolving Needs," *Nature Reviews Clinical Oncology* 19 (2022): 91–113, https://doi.org/10.1038/s41571-021-00565-2.

8. W. D. Foulkes, I. E. Smith, and J. S. Reis-Filho, "Triple-Negative Breast Cancer," *New England Journal of Medicine* 363 (2010): 1938–1948, https://doi.org/10.1056/NEJMra1001389.

9. N. T. Ueno and D. Zhang, "Targeting EGFR in Triple Negative Breast Cancer," *Journal of Cancer* 2 (2011): 324, https://doi.org/10.7150/jca.2.324.

10. B. S. Yadav, P. Chanana, and S. Jhamb, "Biomarkers in Triple Negative Breast Cancer: A Review," *World Journal of Clinical Oncology* 6 (2015): 252, https://doi.org/10.5306/wjco.v6.i6.252.

11. J. M. Martínez, I. Prieto, M. A. J. Ramírez, C. Cueva, F. Alba, and M. Ramírez, "Aminopeptidase Activities in Breast Cancer Tissue," *Clinical Chemistry* 45 (1999): 1797–1802, https://doi.org/10.1093/clinchem/45.10.1797.

12. I. Ranogajec, J. Jakić-Razumović, V. Puzović, and J. Gabrilovac, "Prognostic Value of Matrix Metalloproteinase-2 (MMP-2), Matrix Metalloproteinase-9 (MMP-9) and Aminopeptidase N/CD13 in Breast Cancer Patients," *Matrix Metalloproteinase-9* 29 (2012): 561–569.

13. K. Fukasawa, H. Fujii, Y. Saitoh, et al., "Aminopeptidase N (APN/CD13) is Selectively Expressed in Vascular Endothelial Cells and Plays Multiple Roles in Angiogenesis," *Cancer Letters* 243 (2006): 135–143, https://doi.org/10.1016/j.canlet.2005.11.051.

14. R. A. Ashmun and A. T. Look, "Metalloprotease Activity of CD13/Aminopeptidase N on the Surface of Human Myeloid Cells," *Blood* 75 (1990): 462–469, https://doi.org/10.1182/blood.V75.2.462.462.

15. M. Piedfer, D. Dauzonne, R. Tang, J. N'Guyen, C. Billard, and B. Bauvois, "Aminopeptidase-N/CD13 is a Potential Proapoptotic Target in Human Myeloid Tumor Cells," *The FASEB Journal* 25 (2011): 2831, https://doi.org/10.1096/fj.11-181396.

16. D. C. Taussig, "Hematopoietic Stem Cells Express Multiple Myeloid Markers: Implications for the Origin and Targeted Therapy of Acute Myeloid Leukemia," *Blood* 106 (2005): 4086–4092, https://doi.org/10.1182/blood-2005-03-1072.

17. X. He, Z. Feng, J. Ma, et al., "Bispecific and Split Car T Cells Targeting CD13 and TIM3 Eradicate Acute Myeloid Leukemia," *Blood* 135 (2020): 713–723, https://doi.org/10.1182/blood.2019002779.

18. M. Wickström, R. Larsson, P. Nygren, and J. Gullbo, "Aminopeptidase N (CD13) as a Target for Cancer Chemotherapy," *Cancer Science* 102 (2011): 501–508, https://doi.org/10.1111/j.1349-7006.2010.01826.x.

19. S. A. Amin, N. Adhikari, and T. Jha, "Design of Aminopeptidase N Inhibitors as Anti-Cancer Agents," *Journal of Medicinal Chemistry* 61 (2018): 6468–6490, https://doi.org/10.1021/acs.jmedchem.7b00782.

20. G. Severini, L. Gentilini, and C. Tirelli, "Diagnostic Evaluation of Alanine Aminopeptidase as Serum Marker for Detecting Cancer," *Cancer Biochemistry Biophysics* 12 (1991): 199–204.

21. S. Wang and W. S. El-Deiry, "TRAIL and Apoptosis Induction by TNF-Family Death Receptors," *Oncogene* 22 (2003): 8628–8633, https://doi.org/10.1038/sj.onc.1207232.

22. D. Mérino, N. Lalaoui, A. Morizot, et al., "TRAIL in Cancer Therapy: Present and Future Challenges," *Expert Opinion on Therapeutic Targets* 11 (2007): 1299–1314.

23. C. Falschlehner, C. H. Emmerich, B. Gerlach, and H. Walczak, "TRAIL Signalling: Decisions Between Life and Death," *The International Journal of Biochemistry & Cell Biology* 39 (2007): 1462–1475, https://doi.org/10.1016/j.biocel.2007.02.007.

24. J. Lemke, S. von Karstedt, J. Zinngrebe, and H. Walczak, "Getting TRAIL Back on Track for Cancer Therapy," *Cell Death & Differentiation* 21 (2014): 1350–1364, https://doi.org/10.1038/cdd.2014.81.

25. H. Jun, E. Jang, H. Kim, et al., "TRAIL & EGFR Affibody Dual-Display on a Protein Nanoparticle Synergistically Suppresses Tumor Growth," *Journal of Controlled Release* 349 (2022): 367–378, https://doi.org/10.1016/j.jconrel.2022.07.004.

26. H. Jun, M. Yeo, J. P. Jeon, et al., "CD13-Targeting and TRAIL-Displaying Protein Nanoparticles Effectively Induce Apoptotic Cell Death of Acute Myeloid Leukemia, Prolonging Survival in Mouse Models," *Nano Today* 59 (2024): 102474, https://doi.org/10.1016/j.nantod.2024.102474.

27. Y. Kim, J. Kim, S. Eom, et al., "Protein Nanoparticles Simultaneously Displaying TRAIL and EGFR-Binding Ligands Effectively Induce Apoptotic Cancer Cell Death and Overcome EGFR-TKI Resistance in Lung Cancer," *ACS Applied Materials & Interfaces* 17 (2025): 25139–25151, https://doi.org/10.1021/acsami.5c04021.

28. X. Zhang, W. Meining, M. Fischer, A. Bacher, and R. Ladenstein, "X-Ray Structure Analysis and Crystallographic Refinement of Lumazine Synthase From the Hyperthermophile *Aquifex Aeolicus* at 1.6 Å Resolution: Determinants of Thermostability Revealed From Structural Comparisons," *Journal of Molecular Biology* 306 (2001): 1099–1114, https://doi.org/10.1006/jmbi.2000.4435.

29. H. Choi, B. Choi, G. J. Kim, et al., "Fabrication of Nanoreaction Clusters With Dual-Functionalized Protein Cage Nanobuilding Blocks," *Small* 14 (2018): 1801488, https://doi.org/10.1002/smll.201801488.

30. H. Kim, S. Jin, H. Choi, et al., "Target-Switchable Gd (III)-Dota/Protein Cage Nanoparticle Conjugates With Multiple Targeting Affibody Molecules as Target Selective T1 Contrast Agents for High-Field MRI," *Journal of Controlled Release* 335 (2021): 269–280, https://doi.org/10.1016/j.jconrel.2021.05.029.

31. H. Kim, Y. J. Kang, J. Min, H. Choi, and S. Kang, "Development of an Antibody-Binding Modular Nanoplatform for Antibody-Guided Targeted Cell Imaging and Delivery," *RSC Advances* 6 (2016): 19208–19213, https://doi.org/10.1039/C6RA00233A.

32. H. Choi, M. Yeo, Y. Kang, et al., "Lactate Oxidase/Catalase-Displaying Nanoparticles Efficiently Consume Lactate in the Tumor Microenvironment to Effectively Suppress Tumor Growth," *Journal of Nanobiotechnology* 21 (2023): 5, https://doi.org/10.1186/s12951-022-01762-6.

33. S. G. Park, H. J. Kim, H. B. Lee, et al., "Protein Cage Nanoparticle-Based NK Cell-Engaging Nanodrones (NKeNDs) Effectively Recruit NK Cells to Target Tumor Sites and Suppress Tumor Growth," *Nano Today* 54 (2024): 102075, https://doi.org/10.1016/j.nantod.2023.102075.

34. B. Zakeri, J. O. Fierer, E. Celik, et al., "Peptide Tag Forming a Rapid Covalent Bond to a Protein, Through Engineering a Bacterial Adhesin," *Proceedings of the National Academy of Sciences of the United States of America* 109 (2012): E690–E697.

35. S. C. Reddington and M. Howarth, "Secrets of a Covalent Interaction for Biomaterials and Biotechnology: SpyTag and SpyCatcher," *Current Opinion in Chemical Biology* 29 (2015): 94–99.

36. S. G. Park, H. Kim, H. Jun, S. Y. Choi, E. Kim, and S. Kang, "Directing Ricin-Based Immunotoxins With Targeting Affibodies and KDEL Signal Peptide to Cancer Cells Effectively Induces Apoptosis and Tumor Suppression," *Journal of Nanobiotechnology* 20 (2022): 387, https://doi.org/10.1186/s12951-022-01601-8.

37. S. Eom, S. G. Park, Y. Koo, et al., "*In Situ* Forming and Self-Crosslinkable Protein Hydrogels for Localized Cancer Therapy and Topical Wound Healing," *Journal of Controlled Release* 378 (2025): 460–475, https://doi.org/10.1016/j.jconrel.2024.12.026.

38. S. Eom, H. Jun, E. Kim, D. Min, H. Kim, and S. Kang, "Developing Porous Protein Cage Nanoparticles as Cargo-Loadable and Ligand-Displayable Modular Delivery Nanoplatforms," *ACS Applied Materials & Interfaces* 16 (2024): 58464–58476, https://doi.org/10.1021/acsami.4c14505.

39. H. B. Lee, S. G. Park, H. J. Kim, et al., "CD7-Targeted Cytotoxic Potency of Diphtheria Toxin-and Ricin-Based Immunotoxins in Targeted Therapy for T-Cell Acute Lymphoblastic Leukemia," *Molecular Pharmaceutics* 22 (2025): 3255–3267, https://doi.org/10.1021/acs.molpharmaceut.5c00146.

40. Y. Kim, J. Mun, E. Kim, et al., "Compact Clustering of Highly Oligomerized Anti-DR5 Nanobodies Effectively Drives Apoptotic Cancer Cell Death, Significantly Suppressing Tumor Growth," *Nano Today* 65 (2025): 102834, https://doi.org/10.1016/j.nantod.2025.102834.

41. Q. Guo, X. Li, M.-N. Cui, et al., "Cd13: A Key Player in Multidrug Resistance in Cancer Chemotherapy," *Oncology Research* 28 (2020): 533–540, https://doi.org/10.3727/096504020X15919605976853.

42. D. A. Stewart, Y. Yang, L. Makowski, and M. A. Troester, "Basal-Like Breast Cancer Cells Induce Phenotypic and Genomic Changes in Macrophages," *Molecular Cancer Research* 10 (2012): 727–738, https://doi.org/10.1158/1541-7786.MCR-11-0604.

43. K. J. Chavez, S. V. Garimella, and S. Lipkowitz, "Triple Negative Breast Cancer Cell Lines: One Tool in the Search for Better Treatment of Triple Negative Breast Cancer," *Breast Disease* 32 (2011): 35–48, https://doi.org/10.3233/BD-2010-0307.

44. C. R. Tate, L. V. Rhodes, H. C. Segar, et al., "Targeting Triple-Negative Breast Cancer Cells With the Histone Deacetylase Inhibitor Panobinostat," *Breast Cancer Research* 14 (2012): 1–15, https://doi.org/10.1186/bcr3192.

45. L.-M. Tseng, J.-H. Chiu, C.-Y. Liu, et al., "A Comparison of the Molecular Subtypes of Triple-Negative Breast Cancer Among Non-Asian and Taiwanese Women," *Breast Cancer Research and Treatment* 163 (2017): 241–254, https://doi.org/10.1007/s10549-017-4195-7.

46. A. R. Safa, "C-Flip, a Master Anti-Apoptotic Regulator," *Experimental Oncology* 34 (2012): 176–184.

47. M. Rahman, S. R. Davis, J. G. Pumphrey, et al., "TRAIL Induces Apoptosis in Triple-Negative Breast Cancer Cells With a Mesenchymal Phenotype," *Breast Cancer Research and Treatment* 113 (2009): 217–230, https://doi.org/10.1007/s10549-008-9924-5.

48. M. Vogler, H. Walczak, D. Stadel, et al., "Targeting XIAP Bypasses Bcl-2–Mediated Resistance to TRAIL and Cooperates With TRAIL to Suppress Pancreatic Cancer Growth In Vitro and In Vivo," *Cancer Research* 68 (2008): 7956–7965, https://doi.org/10.1158/0008-5472.CAN-08-1296.

49. D. P. Nair, M. Podgórski, S. Chatani, et al., "The Thiol-Michael Addition Click Reaction: A Powerful and Widely Used Tool in Materials Chemistry," *Chemistry of Materials* 26 (2014): 724–744, https://doi.org/10.1021/cm402180t.

Supporting Information

Additional supporting information can be found online in the Supporting Information section.

Supporting File: mabi70158-sup-0001-SuppMat.pdf.